Self-Calibrated Multiharmonic CO_2 Sensor Using VCSEL for Urban *In Situ* Measurement

Lijuan Lan, Jia Chen, Yingchun Wu, Yin Bai, Xiao Bi, and Yanfang Li

***Abstract*— Greenhouse gases have a significant impact on general global climate change. A self-calibrated multiharmonic measurement system based on tunable diode laser absorption spectroscopy (TDLAS) with wavelength modulation spectroscopy, using the vertical-cavity surface-emitting laser, is developed and applied to measure the CO_2 and H_2O concentrations in the urban areas. The precision of the developed system is evaluated using the Allan variance method, and it is found that the multiharmonic can enhance the precision of the system and the first-to-third harmonics are sufficient to achieve the lowest Allan deviation. To validate its accuracy, comparison experiments with the commercial nondispersive infrared (NDIR) instrument (Li-Cor 840A) are performed and the results demonstrate the high accuracy of the TDLAS system and its consistency with the NDIR instrument. Measurements were carried out in autumn and winter of 2017 in the city center of Munich. The results indicate that the *in situ* measurement of the CO_2 concentration in the downtown area correlates with both natural and anthropogenic activities. Due to its high precision and accuracy, the self-calibrated multiharmonic measurement system has a great potential to further study the emission and distribution of CO_2 in the urban areas.**

***Index Terms*— Carbon dioxide concentration, *in situ* measurement, multiharmonic, self-calibrated, tunable diode laser absorption spectroscopy (TDLAS), vertical-cavity surface-emitting laser (VCSEL), wavelength modulation spectroscopy (WMS).**

I. Introduction

THE total anthropogenic greenhouse gas (GHG) emissions have continued increasing and have affected the climate change in the world during the last 60 years. Carbon dioxide (CO_2), the dominant GHG, comes mainly from the burning of fossil fuel, cement production, and flaring [1]. Research has shown that over 50% of the world population lives in cities and their surrounding urban regions [WHO (2014)], where about 70% of total fossil fuel emission is emitted [UNHabitat (2011)] [2], [3]. Thus, an accurate, compact, portable, and long-term measurement sensor will be urgently needed in the environmental sensing in the future in order to better study the CO_2 distribution near the ground, to real-time measure the CO_2 concentration in all weather conditions, to accurately monitor the source of carbon emission in the urban cities, and to help with the urban pollutant emission modeling and to provide policy supports to the government.

There are many techniques to measure atmospheric CO_2 concentration, but the spectroscopic methodologies are the main methods since they do not contact, quickly respond, and do not interfere with the measured medium [4]. The methodologies can be divided into the satellite measurement, ground-based column measurement, and *in situ* point measurement. However, because of the large observational footprint of the satellite measurements, it is hard to estimate the GHG concentrations in the high spatial resolution [5]–[7]. The EM27/SUN is a miniaturized ground-based tabletop solar-tracking Fourier transform infrared spectrometer that can be employed in urban GHG emission studies in various locations. We have designed a completely automated enclosure for the EM27/SUN and used it to detect the column-averaged GHG concentrations in the urban areas [8], [9]. However, since the instrument utilizes the solar light as the light source, it has limitations in application. For example, the measurement can only be carried out in the presence of sunshine, and thus, concentration data for the rainy days and at night are missing. In addition, the column concentration is the average of the light range between the Earth and the Sun rather than the concentration at the ground level.

Nondispersive infrared (NDIR) and tunable diode laser absorption spectroscopy (TDLAS) are the two common techniques used in the *in situ* point measurement of the CO_2 concentration, and they can detect the emission sources with high precision and sensitivity [10]–[14]. However, NDIR has some disadvantages such as the frequency instability of the optical filter due to the controlling by the piezo, which is susceptible to longtime drift. The researchers must periodically calibrate the accuracy of the instrument. TDLAS is more suited for trace gas monitoring because of the tunable diode laser scans across the absorption line at an extremely small bandwidth, in an order of 1×10^{-3} cm^{-1} or smaller, which is about one-tenth of the absorption linewidth [15]. Vertical-cavity surface-emitting laser (VCSEL) is a laser with low power consumption, wide tuning range, and fast frequency modulation responses than that of the traditional DFB laser [16], [17]. It scans across several absorption lines whose wavelength is more than 10 nm; thus, it can simultaneously measure

Manuscript received March 12, 2018; revised July 12, 2018; accepted July 16, 2018. Date of publication August 29, 2018; date of current version March 8, 2019. This work was supported in part by the Technical University of Munich Institute for Advanced Study through the German Excellence Initiative and the European Union Seventh Framework Program under Grant 291763 and in part by the Program of China Scholarships Council under Grant 201608080018. The Associate Editor coordinating the review process was Dr. Mohamed Abou-Khousa. *(Corresponding author: Jia Chen.)*

L. Lan, J. Chen, Y. Bai, and X. Bi are with the Department of Electrical and Computer Engineering, Technical University of Munich, 80333 Munich, Germany (e-mail: jia.chen@tum.de).

Y. Wu is with the State Key Laboratory of Clean Energy Utilization, Zhejiang University, 310027 Hangzhou, China.

Y. Li is with the Shandong Key Laboratory of Optical Fiber Sensing Technologies, Laser Research Institute of Shandong Sciences Academy, 250014 Jinan, China.

Color versions of one or more of the figures in this paper are available online at http://ieeexplore.ieee.org.

Digital Object Identifier 10.1109/TIM.2018.2863445

a few kinds of gas mediums. Moreover, when applying the wavelength modulation spectroscopy (WMS) to TDLAS, the harmonic signals produced via the lock-in amplifier can effectively remove the laser noise. Thus, WMS can effectively improve sensitivity, precision, and signal-to-noise ratio (SNR) in the harsh environments and in the trace gases measurements [18], [19]. People usually use the second harmonic for gas measurement because of its high SNR in the spectrum center; the other harmonics, especially the odd order harmonics, are always ignored because of their low SNR at the line center. Nevertheless, each harmonic contains useful information about the gas parameters, and using only one or two harmonics would cause loss of the information and reduce the measurement precision. Scientists have studied the multiharmonics for a long time. For example, the first harmonic or the odd order harmonics are applied to recover the absorbance line shape [20], [21]. A convolution model for the harmonic spectra was developed to reconstruct the transmission line using 20–25 harmonic coefficients [22], [23]. In the well-known calibration-free $nf/1f$ method, the first harmonic at the line center is used to eliminate the linear incident light intensities in the even order harmonics and then deduce the gas concentration and temperature [24], [25]. Nonetheless, the first harmonic is a signal that contains the incident light intensity and the residual amplitude modulation (RAM) [26], and utilization of the first harmonic will bring the RAM into the calculation. This parameter should be calibrated before measurement so it is not a completely calibration-free algorithm. Chen *et al.* [27] proposed a calibration-free method, which refers to current to wavelength calibration, for CO sensing using the VCSEL laser. That is, the CH_4 absorption lines are utilized to calibrate the wavelength of the weak CO absorption lines. In the algorithm, the zeroth harmonic is treated as the incident light intensity to normalize the other harmonics. However, they only discussed one single harmonic in the detection.

This paper presents a self-calibrated multiharmonic CO_2 and H_2O measurement system based on TDLAS using the VCSEL laser. The zeroth harmonic is employed to eliminate the incident light intensity in other harmonics. The precision of the system is evaluated by the Allan variance method. It concludes that the multiharmonic with wide tuning range improves the precision for about 2–3 times better than the traditional second harmonic method and that the first-to-third harmonics are optimum to obtain the lowest deviation of 0.02 ppm with 10-min average. Then, a commercial NDIR sensor (Li-Cor 840A) is utilized to verify the accuracy of the system; the outcomes validate the high accuracy of the TDLAS system. Moreover, the self-calibrated feature helps the TDLAS system to get rid of the problems of periodical calibration and long-time drift. To further study the CO_2 concentration in the urban areas, experiments were carried out in autumn and winter of 2017 in the city center of Munich. The results demonstrate that the CO_2 concentration was sensitive to numerous factors, for example, the planetary boundary layer (PBL), the seasons and weather conditions, the vegetation photosynthesis and respiration, and the anthropogenic activities. With the properties of self-calibration, high precision, high accuracy, and *in situ* and real-time measurement, the self-calibrated multiharmonic measurement system can be widely applied in the ground-based CO_2 concentration measurement in the future.

II. Self-Calibrated Multiharmonic Measurement

In WMS, the zeroth harmonic, S_{0f}, approximates to the incident light intensity, I_0, when the absorbance is extremely weak ($<1.0\%$). Under low absorbance conditions, the harmonic signals, S_{nf}, which consist of the gas parameters, can be expressed as follows [25]:

$$S_{nf} = -I_0 c P S(T) L H_n, \quad n = 1, 2, 3 \ldots \tag{1}$$

where c, P [atm], $S(T)$ [cm^{-2}/atm], and L [cm] are gas concentration, gas pressure, line strength, and absorbing path length, respectively. H_n is the nth order Fourier component of the spectral line shape. At the line center, H_n is approximately 0 when n is odd and equals to its maximum when n is even. Since the light intensity and the wavelength are simultaneously tuned by the control current of the laser controller which is always set as a ramp wave, the harmonic signals produced by the lock-in amplifier are always modulated and deformed by the ramp wave. Thus, under extremely weak absorbance condition, the nth harmonic normalized by the zeroth harmonic, $\overline{S_{nf}}$, can be expressed as follows:

$$\overline{S_{nf}} = \frac{S_{nf}}{S_{0f}} = \frac{S_{nf}}{I_0} = -c P S(T) L H_n, \quad n = 1, 2, 3 \ldots \tag{2}$$

When I_0 is eliminated, the harmonics are absolute signals and linearly proportional to the gas parameters. Therefore, under given pressure and temperature, the gas concentration can be determined without calibration:

$$c = -\frac{\overline{S_{nf}}}{P S(T) L H_n}, \quad n = 1, 2, 3 \ldots \tag{3}$$

In the measurement system, we can develop a lock-in amplifier that produces all harmonics simultaneously, and then, the zeroth harmonic is applied to eliminate the incident light intensity in other harmonics. The normalized harmonics are obtained, and the gas concentration can subsequently be inferred according to (3). There is no additional reference installation throughout the entire process so that it is a self-calibrated method to measure the gas concentration. The linear least square curve fitting (LLSCF) algorithm is utilized to infer the gas concentration as follows [23], [28]:

$$\hat{C} = -\frac{1}{P S(T) L} (\Psi^T \Psi)^{-1} \Psi^T Y \tag{4}$$

where Ψ is the observation matrix, including multiple Fourier components for different gas species, the offset, and the normalized RAM; Y is a vector for the selected multiple harmonic signals; and $\hat{C} = (c_1, c_2, \ldots, l_O, l_R)^T$ is the optimum solved vector that contains the concentrations of different gas species, the levels of the offset, and the RAM. Equation (4) is a closed, convergent, and fast computing expression from which the gas concentrations of different multiharmonic combinations can be calculated. The LabVIEW data processing interface of the LLSCF algorithm for real-time CO_2 and H_2O concentrations measurement is shown in Fig. 2.

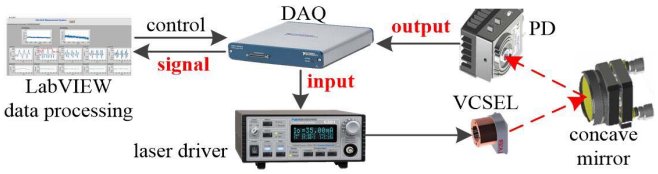

Fig. 1. Experimental setup for concentration measurement.

TABLE I

ABSORPTION SPECTRAL PARAMETERS NEAR 2004 NM FOR CO_2 AND H_2O ABSORPTION LINES

Index	I_H_2O	I_CO_2	II_CO_2	III_CO_2
Wavelength (nm)	2002.829	2002.998	2003.503	2004.019
Line strength(cm^{-1} /(molec·cm^{-2}))	5.09e-23	1.21e-21	1.26e-21	1.29e-21

III. EXPERIMENTAL SYSTEM

A. Experimental Setup

The experimental setup is shown in Fig. 1. A VCSEL (VL-2004-1-SQ-A5) is used as the spectroscopic source whose center wavelength is 2004 nm. The laser wavelength is controlled by a laser diode controller (Arroyo Instruments 6301). A concave mirror with a focal length of 75 mm reflects the laser light back to the detector and doubles the path length to 30 cm, as shown in Fig. 1. The optical power is detected by an InGaAs amplified detector (PDA10DT-EC). Then, the detector signals are recorded by a high-speed memory data acquisition (DAQ) card (NI USB-6361) and demodulated using a digital lock-in amplifier (LabVIEW). The DAQ also works as a signal generator that provides the low-frequency ramp signal (10 Hz) and high-frequency sinusoidal signal (6 kHz) to tune and modulate the laser wavelength. A sensor using a Raspberry Pi system is set nearby to simultaneously measure pressure and temperature.

The data processing of the experiment is a LabVIEW program that contains three sections: signal controller, lock-in amplifier, and concentration measurement. The signal controller produces the ramp (1.2 V and 10 Hz) and sinusoidal signals (60 mV and 6 kHz) as the control current to tune and modulate the laser wavelength. The digital lock-in amplifier produces the zeroth-to-fifth harmonics of the detected signal. All harmonics are normalized by the zeroth harmonic, which approximates to the incident laser intensity when the absorbance is low. The third part is the concentration measurement. First, the peak values of each absorption line in the second harmonic are sought as the line centers. Then, the relationship between the ramp signal and the wavelength can be determined. Finally, all the harmonics are selected for different combinations to calculate the gas concentrations with 0.1-s measurement rates based on the LLSCF algorithm.

Fig. 2 shows the LabVIEW interface for the CO_2 and H_2O concentrations measurement. That is, the curve fitting results of the first-to-fifth harmonics with one H_2O absorption line and three CO_2 absorption lines near 2004 nm are shown in the graphs. The spectral parameters from HITRAN are listed in Table I [29]. Fig. 2 demonstrates that the harmonics of I_H_2O are overlapped with the harmonics of I_CO_2 absorption line under atmospheric pressure when the Lorentzian line shape is dominant. In the following subsection B, experiments are taken to validate that the curve fitting algorithm can help to overcome the problem of overlapping lines, and the precision of the self-calibrated multiharmonic method with different scanning scopes. The scopes include single absorption line (II_CO_2), double absorption lines (II_CO_2 and III_CO_2), and three CO_2 absorption lines with one H_2O absorption line (I_H_2O, I_CO_2, II_CO_2, and III_CO_2).

B. Precision of the System

Allan variance is a method of measuring the frequency stability of the measurement system in the time domain [30], [31]. This method can be used to determine the intrinsic noise in a system as a function of the integrating time. It is one of the most popular methods for identifying and quantifying the different noise terms that exist in the inertial sensor data. The Allan variance analysis consists of computing its square root as a function of a different integrating time and then analyzing the characteristic regions and double logarithmic scale slope of the Allan deviation (σ_{Allan}) curves to identify the different noise modes. As shown in Fig. 3, the white noise is dominant when the slope is -0.5 (dashed line) and the Brownian noise is dominant when the slope is 0.5 (dotted line). When σ_{Allan} is minimum ($\sigma^{\min}_{\text{Allan}}$), the optimum integrating time (τ_{opt}) and the detection limit is determined. Allan deviation plots of the TDLAS multiharmonic CO_2 concentration measurement are indicated in Figs. 3 and 4 and Table II.

Fig. 3 shows the Allan plots of the CO_2 concentration results using the first, second, and third harmonics with different ranges of scanning wavelengths. It can be seen that in the range dominated by the white noise, the precision of the single absorption line is lower than that of the double and the triple absorption lines. For example, at 1.0 s, σ_{Allan} of the second harmonic with single absorption line is 1.3 ppm, while with double and triple absorption lines, it can obtain at about 1.0 ppm, suggesting that broadening the scanning range helps to cut down the white noise. For the second-harmonic detection as listed in Table II, the three absorption lines obtain the lowest $\sigma^{\min}_{\text{Allan}}$ at 0.05 ppm with 400 s averaged. The above-mentioned results can be summed up by observing that a wide scanning range of wavelengths effectively reduces the white noise and the Brownian noise, and improves the optimum integrating time. For the Allan curves of the first, second, and third harmonics with three CO_2 absorption lines, we can learn that the higher order the harmonic is, the larger the deviations are. That is, the first harmonic has the lowest white noise. For instance, at 1 min, they are 0.1, 0.12, and 0.18 ppm for the first, second, and third harmonics, respectively. Hangauer *et al.* [23] concluded that the second harmonic had better noise performance than the first harmonic which was different from our results. It is because they approximated the RAM in the first harmonic as a slope, which reduced the precision of the first-harmonic detection.

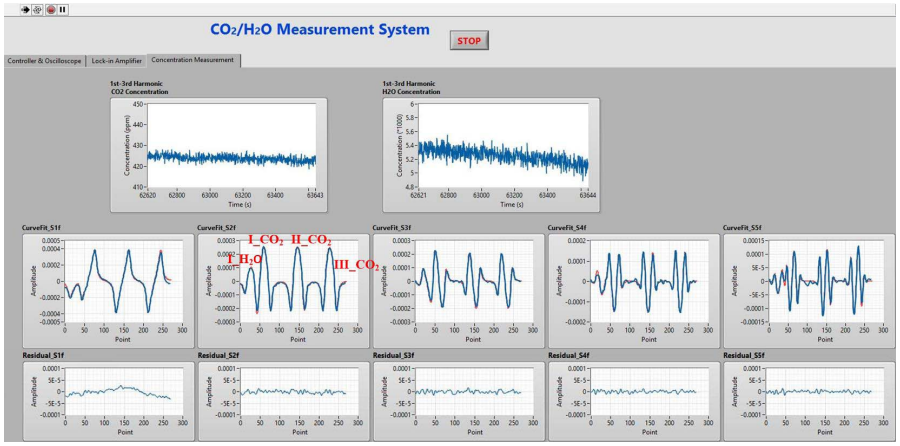

Fig. 2. LabVIEW data processing interface. The top two graphs are the concentrations of CO_2 and H_2O. The middle five graphs are the experimental harmonics (blue lines) and the LLSCF results (red lines) from the first to fifth harmonics. The bottoms are the residuals between the experimental and the LLSCF results. The residual amplitudes are less than one-tenth of their relative harmonics, indicating the high reliability of the LLSCF algorithm. The notations of each absorption lines are marked in the second harmonics.

TABLE II

OVERVIEW AND COMPARISONS OF THE ALLAN ANALYSIS FOR THE MULTIHARMONIC DETECTIONS

Groups	Lines n.	Harm. n.	σ_{Allan}(ppm)@1s	σ_{Allan}(ppm)@1min	$\sigma^{\text{min}}_{\text{Allan}}$(ppm)@$\tau_{\text{opt}}$(s)(Absorbance)
II_CO_2	1	2	1.27	0.16	0.08@500(3.24×10^{-7})
II_CO_2&III_CO_2	2	2	1.04	0.13	0.06@400(2.43×10^{-7})
2^{nd} harm.	3	2	0.97	0.12	0.05@400(2.02×10^{-7})
1^{st} harm.	3	1	0.72	0.10	0.03@800(1.21×10^{-7})
3^{rd} harm.	3	3	1.27	0.18	0.09@200(3.64×10^{-7})
2^{nd}-3^{rd} harm.	3	2,3,	0.77	0.10	0.05@200(2.02×10^{-7})
2^{nd}-5^{th} harm.	3	2,3,4,5	0.67	0.09	0.04@300(1.62×10^{-7})
1^{st}-3^{rd} harm.	3	1,2,3	0.52	0.07	0.02@600(8.09×10^{-8})
1^{st}-5^{th} harm.	3	1,2,3,4,5	0.49	0.07	0.02@600(8.09×10^{-8})

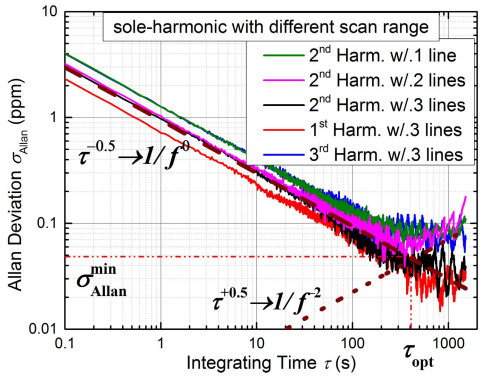

Fig. 3. Allan plots of sole harmonic detection with one, two, and three absorption lines. The dashed and dotted lines indicate the white and Brownian noises, respectively. τ_{opt} is the time when σ_{Allan} is minimum ($\sigma^{\text{min}}_{\text{Allan}}$).

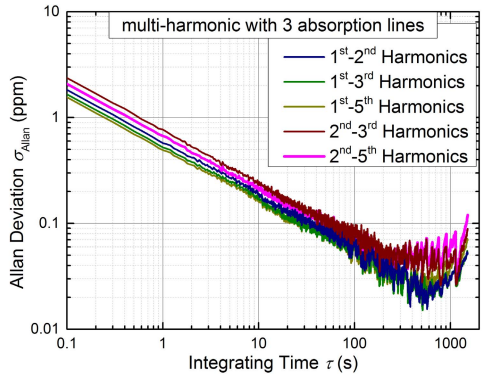

Fig. 4. Allan plots of different multiharmonic combinations with three absorption lines.

Allan plots for different multiharmonic combinations using three CO_2 absorption lines are shown in Fig. 4. Compared with the Allan plots of sole harmonic in Fig. 3, the measurement precisions of multiple harmonics are effectively improved. For example, the deviations of the first and the second harmonics are 0.7 and 1.0 ppm at 1 s, respectively, while the lowest deviation of the multiharmonic is 0.5 ppm at the same integrating time. Second, the Allan deviations of the multiple harmonics, which contain the first harmonic, have lower values than those without the first harmonic. The precision can be improved when the first harmonic is employed in the measurement because the first harmonic has the highest precision according to the aforementioned discussion (see Fig. 3). Third, the more harmonics are used, the higher the precision that can be obtained in the measurement. However, the Allan plots of the first-to-third harmonics and the first-to-fifth harmonics are very similar and both obtain the highest precision of 0.02 ppm at 10 min corresponding to absorbance in an order of 1×10^{-8}. Because wide scanning of three absorption lines supports sufficient data for concentration calculation, the first-to-third harmonics have already gained the highest precision in measurement. More harmonics than

this optimal value can no longer improve the precision in the application of up to three absorption lines scanning.

Overall, the wide wavelength scanning and multiharmonic heighten the precision because more useful data are utilized in measurement. The higher the harmonic order, the lower the precision. That is, the first harmonic has the highest precision when compared with the second and third harmonic measurements. In the multiharmonic detection, the series which includes the first harmonic has lower σ_{Allan} than that without the first harmonic. And the precision of the system can be improved for about 2–3 times when compared with the sole second-harmonic detection. More harmonics can obtain higher precision, but the first-to-third harmonics are sufficient to achieve the highest precision when three absorption lines are employed for scanning, and more than the first three harmonics do not further enhance the precision of the measurement system.

C. Accuracy of the System

The above-mentioned experimental results have verified the high precision of the self-calibrated multiharmonic measurement system. In this section, the comparison experiments are implemented to validate its accuracy, where the commercial NDIR sensor (Li-Cor 840A CO_2/H_2O gas analyzer) is served as a calibration standard instrument. The NDIR sensor uses a continuous broadband infrared lamp as the light source, and the light passes through the measured gas and is recorded by a photodetector, in front of which there is a light filter that can eliminate the useless wavelengths. The gas concentration is deduced based on the Beer–Lambert law. The measurement range of CO_2 is 0–20 000 ppm with less than 1 ppm signal noise at 370 ppm. And the H_2O range is 0‰-60‰ with 0.01‰ at 10‰ of noise level, with a measurement recording rate of 1 s. This instrument has high accuracy over the whole measurement range because of its automatic temperature and pressure compensations but it must be calibrated periodically.

Measurements are carried out to validate the accuracy of the TDLAS system. The gas tube of the NDIR sensor is set close to the optical path of TDLAS, thus the gas concentrations in both systems are the same. When starting the measurements, these two sensors work simultaneously and independently to acquire the concentrations of CO_2 and H_2O. Fig. 5 shows the experimental results of CO_2 and H_2O concentrations based on NDIR and TDLAS which were implemented in the city center from September 16 to 18, 2017. For the TDLAS measurement, the outcomes are retrieved from the first-to-third harmonics with 1-min average for which σ_{Allan} is 0.07 ppm for CO_2 concentration, as shown in Fig. 4.

Fig. 5(a) shows the variation of CO_2 concentration on the ground level, where the maximum concentration occurs in the morning at about 430 ppm while the lowest point happens at around 17:00 at nearly 380 ppm. The measured days were partly cloudy with sunrises and sunsets at 06:53 and 19:21 (UTC+2), respectively. The trend of CO_2 concentration is reasonable because the PBL is shallow at night and deep during the day due to solar heating of the ground surface,

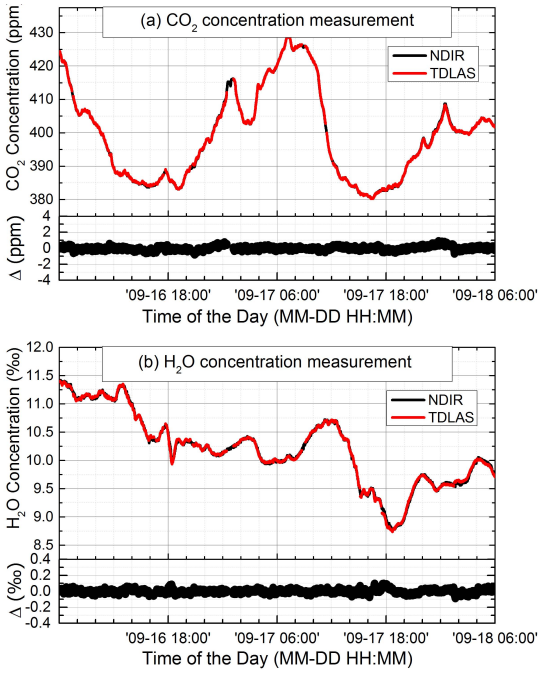

Fig. 5. Measurement of the CO_2 and H_2O concentrations based on the NDIR and the TDLAS systems averaged at 1 min.

leading to the CO_2 concentration increasing at night and decreasing in the day [3], [32]. Moreover, the vegetation photosynthesis uptakes CO_2 near the surface, making the CO_2 concentration to decrease below the average concentration, around 406 ppm [8], in the daytime, and the increment of CO_2 concentration at night is partly caused by the biosphere respiration. The integrative effects of the PBL and the photosynthesis and respiration result in the distinctive variation of CO_2 concentration throughout the day. For comparisons, the NDIR and TDLAS systems have similar results in the whole period. The bottom graph is the concentration residual between these two systems, where the differences are within 2 ppm, indicating that the TDLAS system has the same level accuracy as the NDIR sensor in measuring CO_2 concentration. Fig. 5(b) shows the H_2O concentration measured simultaneously with the CO_2 concentration. These two systems also have the same H_2O results with residuals within 0.2‰, showing the same high consistency for measuring H_2O concentration as that of CO_2 concentration.

The comparison experiments between NDIR and TDLAS are taken at a wider concentrations range. The results are represented as the linear regressions in Fig. 6, where the regression ranges are 380–540 ppm for CO_2 concentration and 4‰–13.5‰ for H_2O concentration. The R squares, the intercepts, and the slopes of the linear regressions are approximately 0.999, 0, and 1, respectively, demonstrating that the TDLAS sensor has high accuracy and high consistency with the commercial NDIR instrument in measuring the CO_2 and H_2O concentrations. It is worth mentioning that the harmonic signals of CO_2 and H_2O near 2003 nm are overlapped, as shown in Fig. 2 and Table I. The experimental results show that the self-calibrated multiharmonic system

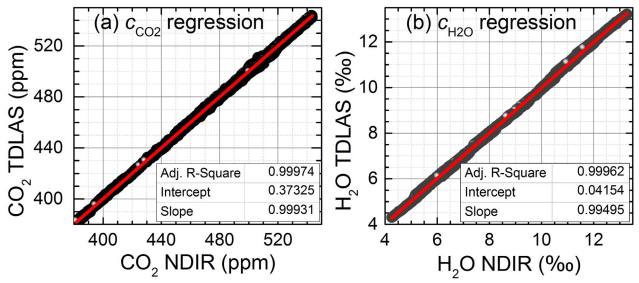

Fig. 6. Linear regressions of the CO_2 and H_2O concentration measurements between the NDIR and the TDLAS systems.

based on the LLSCF algorithm can overcome the spectrum's overlapping and yield a highly accurate measurement of gas concentration.

IV. Application in Urban Area Measurement

As presented in Fig. 7, the self-calibrated multiharmonic measurement system was operated in autumn and winter of 2017 to study the CO_2 concentration variation in the urban area. The system is located on the second floor of a laboratory at Theresienstrasse, Munich. The windows of the room are open to ensure the same CO_2 concentrations indoor and outdoor. The measurements are carried out without interference. The heating system is opertated in winter to make the room to be drier than the outer environment, thus we do not analyze the H_2O concentration in this section. The measurement data were obtained from the same multiharmonics as that given in Fig. 5, in which the weather conditions and anthropogenic activities are also indicated in the graphs. The situations of the measurements are as follows: the black curve in Fig. 7(a) is the TDLAS experimental data from Fig. 5(a). The red line in Fig. 7(b) was measured from September 23 to 25, 2017. In general, the sunshine duration was nearly 12 h on these days, from 07:03 to 19:07 (UTC + 2). The solid line in Fig. 7(c) was measured from December 23 to 25, 2017. The blue curve in Fig. 7(d) was run from the last day of 2017 to the second day of 2018. The sun rose at 08:04 and set at 16:29 (UTC + 1) with the shortest daytime of the entire year.

Some interesting findings can be seen in the experiments. First, a noticeable tendency during the day and night, that is, the CO_2 concentration in the urban area decreases in the day and increases at night, is observed in September in Fig. 7(a) and (b). The large fluctuations are caused by the synergies of the PBL and the vegetation photosynthesis and respiration which are still very active in autumn, as explained earlier. The peak and bottom values happen at around 10:00 am and 17:00 pm, which are also verified by other researchers [33], [34]. The lowest concentration in daytime can decrease to 380 ppm. During the night, the maximum value can reach 430 ppm or even more due to the shallow PBL and the CO_2 accumulation from vegetation respiration and anthropogenic activities, which will be discussed in the following.

Fig. 7(c) and (d) shows the CO_2 concentration obtained in winter with the shortest sunshine duration and the lowest temperature of the entire year. We can learn that there is no discernible variation or substantial increment and decrement during the day and night. Compared with the curve in Fig. 7(a) fluctuating between 380 and 430 ppm, the variation ranges shown in Fig. 7(c) and (d) are much narrower, only vary from 405 to 420 ppm. In winter, the temperature in the atmosphere is about 0 °C and the shortest daytime is 8.4 h, and the PBL is thin to several hundred meters and does not change a lot between day and night because the solar heating is weak. The animals and plants are mostly in hibernation, with little photosynthesis and little respiration, which means no much CO_2 uptake or release from the biosphere. Therefore, the major contributor to the CO_2 concentration in the downtown area is the human activities. The CO_2 is gathered in a limited space causing higher concentration and smaller variation during the whole day than that of the autumn data. The minimum concentration in Fig. 7(c) and (d) is above 400 ppm which approximates to the atmospheric average value.

Third, the weather conditions have great impacts on the CO_2 concentration in the city center. When the meteorology is unfavorable to air diffusion, such as fog, rain, or cloudy days without wind, the CO_2 concentration in urban areas will increase quickly. For example, the red line has the peak values of more than 460 ppm which is mainly attributed to the rain and fog as demonstrated in Fig. 7(b). The line in Fig 7(c), which increases to 420 ppm in the last minutes, is caused by the fog. On the contrary, when the meteorological term contributes to gas diffusion, the CO_2 concentration will noticeably decline. There were strong winds at around 04:00 of the 1st and midnight of the 2nd in January as shown in 7(d), and the CO_2 concentration dropped measurably from 420 to 405 ppm.

Finally, the human activities also play an important role in the CO_2 concentration variation. Considering the curves in Fig. 7(b), where the dashed line is the experimental results of Fig. 7(a), it is obvious that the red line has higher values than the dashed line among the whole measurement. This is because the well-known solemn celebration of the folk festival, called Oktoberfest, is held during this period every year in Munich. The celebration attracts millions of international tourists gathering in this city to celebrate the annual unprecedented days at Theresienwiese, which is only 2 km away from the monitoring site. The high concentration of the red line is mainly caused by the surging tourists. For another example in Fig. 7(d) during the New Year's Eve, many fireworks were ignited by the citizens to celebrate the arrival of 2018, which led to a CO_2 peak at midnight of the New Year. After the fireworks died down, the concentration decreased from 440 to 420 ppm in 30 min, implying the significant effect of the anthropogenic activities.

The above-mentioned measurements have illustrated the factors that can affect the ground-based CO_2 concentration as follows: the PBL, the vegetation photosynthesis and

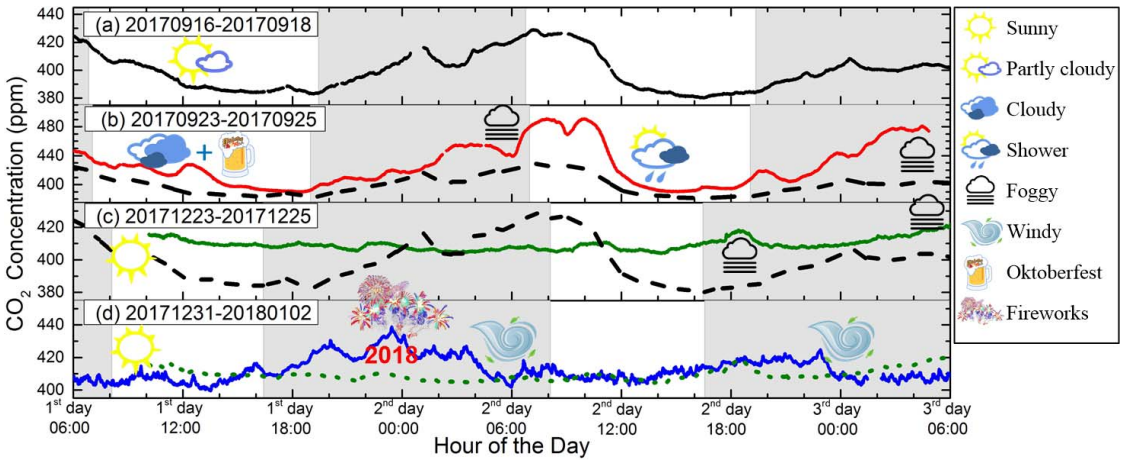

Fig. 7. Measurements of the CO_2 concentration in four periods based on TDLAS and averaged over 1 min, where the gray parts in the graphs represent the night time. (a) Measured from September 16–18, 2017. (b) Obtained from September 23–25, 2017. (c) Outcomes from December 23–25, 2017. The black-dashed lines in (b) and (c) represent the experimental results of (a). (d) Acquired from December 31, 2017 through January 2, 2018, where the green-dotted line is the data in (c). As displayed in (d), the peak value occurred at the beginning of the second day because the fireworks are lit to celebrate the coming of 2018.

respiration, the seasons and weather conditions, and, most importantly, the anthropogenic activities. Thus, to better study the CO_2 concentration distribution in the urban areas, a real-time measurement instrument with high precision, accuracy, sensitivity, and stability is urgently needed in the future, and the experimental results have demonstrated that the self-calibrated multiharmonic measurement system is a potential sensor in the applications.

V. Conclusion

A self-calibrated multiharmonic measurement system has been developed to measure the CO_2 and H_2O concentrations based on TDLAS using the VCSEL laser. According to the Allan analysis, wide wavelength scanning and multiharmonics can improve the precision for about 2–3 times in measurement when compared with the traditional second-harmonic detection. The first-to-third harmonics with up to three CO_2 absorption lines are optimal to obtain the best noise level. The experimental comparisons were made between the TDLAS measurement system and the commercial NDIR sensor to validate the accuracy of the TDLAS system. The linear regressions of CO_2 and H_2O measurements have indicated the high consistency of the two sensors. The measurements were performed in autumn and winter 2017 in the city center which displayed that the daily tendency of the ground-based CO_2 concentration was influenced by numerous factors, such as the PBL, the vegetation photosynthesis and respiration, the seasons and weather conditions, and the anthropogenic activities.

This paper demonstrates high precision and accuracy of the self-calibrated multiharmonic measurement system. Moreover, the sensor is suited for the *in situ* measurements of GHGs in an urban network with high spatial coverage, given its properties of self-calibration, fast and real-time measurement, and low power consumption.

Acknowledgment

The authors would like to thank Vertilas GmbH for providing the vertical-cavity surface-emitting laser in the tunable diode laser absorption spectroscopy measurement system and J. Rosskopf for the technical consultation. They would also like to thank S. Ye and M. Wenig from the Ludwig Maximilian University of Munich for providing the Li-Cor 840A CO_2/H_2O gas analyzer and the weather data during the measurement periods, and P. Zhou and Z. Peng from Tsinghua University, Beijing, China, for supporting assistance on designing the digital lock-in amplifier.

References

[1] Core Writing Team, R. K. Pachauri, and L. A. Meyer, Eds., "Contribution of working groups I, II and III to the fifth assessment report of the intergovernmental panel on climate change," Intergovernmental Panel on Climate Change, Geneva, Switzerland, Synth. Rep., 2014, p. 151. [Online]. Available: http://www.ipcc.ch/report/ar5/syr/

[2] F. Bréon *et al.*, "An attempt at estimating Paris area CO_2 emissions from atmospheric concentration measurements," *Atmos. Chem. Phys.*, vol. 15, no. 4, pp. 1707–1724, 2015.

[3] K. McKain, S. C. Wofsy, T. Nehrkorn, J. Eluszkiewicz, J. R. Ehleringer, and B. B. Stephens, "Assessment of ground-based atmospheric observations for verification of greenhouse gas emissions from an urban region," *Proc. Nat. Acad. Sci. USA*, vol. 109, no. 22, pp. 8423–8428, 2012.

[4] L. J. Lan, Y. J. Ding, Z. M. Peng, Y. J. Du, and Y. F. Liu, "Calibration-free wavelength modulation for gas sensing in tunable diode laser absorption spectroscopy," *Appl. Phys. B*, vol. 117, no. 4, pp. 1211–1219, 2014.

[5] A. Liang, W. Gong, and G. Han, "OCO-2 XCO_2 validation using TCCON data," in *Proc. IEEE Int. Geosci. Remote Sens. Symp. (IGARSS)*, Jul. 2016, pp. 830–833.

[6] V. Velazco *et al.*, "Towards space based verification of CO_2 emissions from strong localized sources: Fossil fuel power plant emissions as seen by a CarbonSat constellation," *Atmos. Meas. Techn.*, vol. 4, no. 12, pp. 2809–2822, 2011.

[7] J. Heymann *et al.*, "Consistent satellite XCO_2 retrievals from SCIAMACHY and GOSAT using the BESD algorithm," *Atmos. Meas. Tech.*, vol. 8, no. 7, pp. 2961–2980, 2015.

[8] J. Chen *et al.*, "Differential column measurements using compact solar-tracking spectrometers," *Atmos. Chem. Phys.*, vol. 16, no. 13, pp. 8479–8498, 2016.

[9] L. Heinle and J. Chen, "Automated enclosure and protection system for compact solar-tracking spectrometers," *Atmos. Meas. Techn.*, vol. 11, no. 4, pp. 2173–2185, 2018.

[10] F. Jin *et al.*, "*In situ* measurement of atmospheric carbon dioxide at Yanbian, China: Estimating its northeast Asian emission regions," *Sci. China Earth Sci.*, vol. 55, no. 10, pp. 1742–1754, 2012.

[11] T. Yasuda, S. Yonemura, and A. Tani, "Comparison of the characteristics of small commercial NDIR CO_2 sensor models and development of a portable CO_2 measurement device," *Sensors*, vol. 12, no. 3, pp. 3641–3655, 2012.

[12] Y. Meng *et al.*, "A modified empirical mode decomposition algorithm in TDLAS for gas detection," *IEEE Photon. J.*, vol. 6, no. 6, pp. 1–7, Dec. 2014.

[13] C. Liu, L. Xu, Z. Cao, and H. McCann, "Reconstruction of axisymmetric temperature and gas concentration distributions by combining fan-beam TDLAS with onion-peeling deconvolution," *IEEE Trans. Instrum. Meas.*, vol. 63, no. 12, pp. 3067–3075, Dec. 2014.

[14] C. Brosy *et al.*, "Simultaneous multicopter-based air sampling and sensing of meteorological variables," *Atmos. Meas. Tech.*, vol. 10, no. 8, pp. 2773–2784, 2017.

[15] F. J. Duarte, *Tunable Lasers Handbook*. Amsterdam, The Netherlands: Elsevier, 1996.

[16] A. Hangauer, J. Chen, R. Strzoda, and M.-C. Amann, "The frequency modulation response of vertical-cavity surface-emitting lasers: Experiment and theory," *IEEE J. Sel. Topics Quantum. Electr.*, vol. 17, no. 6, pp. 1584–1593, Nov./Dec. 2011.

[17] Y. Wang *et al.*, "Tunable diode laser absorption spectroscopy-based detection of propane for explosion early warning by using a vertical cavity surface enhanced laser source and principle component analysis approach," *IEEE Sensors J.*, vol. 17, no. 15, pp. 4975–4982, Aug. 2017.

[18] J. Reid and D. Labrie, "Second-harmonic detection with tunable diode lasers—Comparison of experiment and theory," *Appl. Phys. B*, vol. 26, no. 3, pp. 203–210, 1981.

[19] J. Chen, A. Hangauer, R. Strzoda, and M.-C. Amann, "Laser spectroscopic oxygen sensor using diffuse reflector based optical cell and advanced signal processing," *Appl. Phys. B*, vol. 100, no. 2, pp. 417–425, 2010.

[20] G. Stewart, W. Johnstone, J. R. P. Bain, K. Ruxton, and K. Duffin, "Recovery of absolute gas absorption line shapes using tunable diode laser spectroscopy with wavelength modulation—Part I: Theoretical analysis," *J. Lightw. Technol.*, vol. 29, no. 6, pp. 811–821, Mar. 15, 2011.

[21] Z. Peng, Y. Ding, L. Che, and Q. Yang, "Odd harmonics with wavelength modulation spectroscopy for recovering gas absorbance shape," *Opt. Express*, vol. 20, no. 11, pp. 11976–11985, 2012.

[22] A. Hangauer, J. Chen, and M.-C. Amann, "Modeling of the n-th harmonic spectra used in wavelength modulation spectroscopy and their properties," *Appl. Phys. B*, vol. 90, no. 2, pp. 249–254, 2008.

[23] A. Hangauer, J. Chen, R. Strzoda, and M.-C. Amann, "Multi-harmonic detection in wavelength modulation spectroscopy systems," *Appl. Phys. B*, vol. 110, no. 2, pp. 177–185, 2013.

[24] H. Li, G. B. Rieker, X. Liu, J. B. Jeffries, and R. K. Hanson, "Extension of wavelength-modulation spectroscopy to large modulation depth for diode laser absorption measurements in high-pressure gases," *Appl. Opt.*, vol. 45, no. 5, pp. 1052–1061, Feb. 2006.

[25] Z. Peng, Y. Ding, L. Che, X. Li, and K. Zheng, "Calibration-free wavelength modulated TDLAS under high absorbance conditions," *Opt. Express*, vol. 19, no. 23, pp. 23104–23110, 2011.

[26] J. T. C. Liu, J. B. Jeffries, and R. K. Hanson, "Wavelength modulation absorption spectroscopy with 2 f detection using multiplexed diode lasers for rapid temperature measurements in gaseous flows," *Appl. Phys. B*, vol. 78, nos. 3–4, pp. 503–511, 2004.

[27] J. Chen, A. Hangauer, R. Strzoda, and M. Amann, "VCSEL-based calibration-free carbon monoxide sensor at 2.3 μm with in-line reference cell," *Appl. Phys. B*, vol. 102, no. 2, pp. 381–389, 2011.

[28] A. Savitzky and M. J. E. Golay, "Smoothing and differentiation of data by simplified least squares procedures," *Anal. Chem.*, vol. 36, no. 8, pp. 1627–1639, 1964.

[29] L. S. Rothman *et al.*, "The *HITRAN* 2008 molecular spectroscopic database," *J. Quant. Spectrosc. Radiat. Transf.*, vol. 110, nos. 9–10, pp. 533–572, 2009.

[30] D. W. Allan, "Statistics of atomic frequency standards," *Proc. IEEE*, vol. 54, no. 2, pp. 221–230, Feb. 1966.

[31] P. Werle, R. Mücke, and F. Slemr, "The limits of signal averaging in atmospheric trace-gas monitoring by tunable diode-laser absorption spectroscopy (TDLAS)," *Appl. Phys. B*, vol. 57, no. 2, pp. 131–139, 1993.

[32] R. Stull, *An Introduction to Boundary Layer Meteorology*, vol. 13. London, U.K.: Springer, 2012.

[33] J. Moore and A. D. Jacobson, "Seasonally varying contributions to urban CO_2 in the Chicago, Illinois, USA region: Insights from a high-resolution CO_2 concentration and $\delta^{13}C$ record," *Elementa, Sci. Anthropocene*, vol. 3, no. 000052, 2015.

[34] J. Xu *et al.*, "Interpreting the $^{13}C/^{12}C$ ratio of carbon dioxide in an urban airshed in the Yangtze River Delta, China," *Atmos. Chem. Phys.*, vol. 17, no. 5, pp. 3385–3399, 2017.

Lijuan Lan received the B.Sc. degree in precision instrument and the M.Eng. degree in thermal engineering from Tsinghua University, Beijing, China, in 2012 and 2015, respectively. She is currently pursuing the Ph.D. degree in environmental sensing and modeling with the Technical University of Munich, Munich, Germany.

Her current research interests include the greenhouse gases detection based on optical techniques.

Jia Chen received the Diploma degree from the Karlsruhe Institute of Technology, Karlsruhe, Germany, in 2006, and the Ph.D. degree from the Technical University of Munich (TUM), Munich, Germany, in 2011.

From 2011 to 2015, she was a Post-Doctoral Fellow with the Environmental Science and Engineering Department, Harvard University, Cambridge, MA, USA. In 2015, she was appointed as a Professor at TUM, where she is currently the Head of the Environmental Sensing and Modeling Group, Department of Electrical and Computer Engineering. She holds an associate position at the Department of Earth and Planetary Sciences, Harvard University. She has authored and co-authored 30 peer-reviewed journals and 70 conference publications.

Yingchun Wu received the B.Sc. degree from the University of Science and Technology of China, Hefei, China, in 2009, and the Ph.D. degree from Zhejiang University, Hangzhou, China, in 2014.

From 2014 to 2017, he was a Post-Doctoral Researcher at CORIA, CNRS, Saint-Étienne-du-Rouvray, France, the Department of Electrical and Computer Engineering, Technical University of Munich, Munich, Germany, and the School of Computing, Engineering and Mathematics, University of Brighton, Brighton, U.K.. He is currently a Researcher with the School of Energy Engineering, Zhejiang University. His current research interests include the optical measurement of reacting multiphase flow, including absorption spectroscopy, digital holography, rainbow refractometry, and light scattering techniques.

Yin Bai received the B.Sc. degree from Tsinghua University, Beijing, China, and the Ph.D. degree from the University of Chinese Academy of Sciences, Beijing.

She is currently a Post-Doctoral Fellow with the Environmental Sensing and Modeling Group, Technical University of Munich, Munich, Germany. Her current research interests include the development of electrochemical microsensors for water environment monitoring, traffic speed metrology, and the development of compact optical sensors for atmosphere pollutants monitoring.

Xiao Bi received the B.Sc. degree in electrical engineering from the University of Siegen, Siegen, Germany, in 2015, and the M.Sc. degree in power engineering from the Technical University of Munich, Munich, Germany, in 2018.

Since 2017, he has been contributing to research about environmental pollutant sensing and gas detection.

Yanfang Li received the B.Sc. and M.Eng. degrees from the Control Science and Engineering School, Shandong University, Jinan, China, in 2003 and 2006, respectively.

Since 2006, she has been with the Laser Research Institute of Shandong Sciences Academy, Jinan, where she is currently an Associate Research Fellow. Her current research interests include gas detection, chemical industry safety, and atmospheric state monitoring.